RIPARIAN MICROTOPOGRAPHY OF SHONAI RIVER BY APPLYING POLE-CAMERA METHOD

RYOSUKE AKAHORI
Aichi Institute of Technology, Toyota, Japan, rakahori@aitech.ac.jp

ABSTRACT

Currently, structures from motion-multi view stereo (SfM-MVS) techniques are widely used and considered to be among the most powerful tools for capturing the surface topography of riparian environments. Majority of the original images processed using the SfM-MVS technique are acquired through unmanned aerial vehicles (UAVs) because of their portability and operational feasibility. However, the current legal environment for UAV operation has globally changed due to security reasons, and restricted areas for UAV operation are expected to consistently expand hereafter. In this study, an alternative method to capture images for the SfM-MVS is proposed, in which a remote-controlled camera mounted on top of a 7-m telescopic pole is used, referred to as the pole-camera method. We applied the proposed method during our field observations of the Shonai River, located in Japan, to investigate the evolution of microtopography and the riparian herbaceous vegetation in a specific reach of this river. High-resolution digital surface models (DSM) were produced as a result of SfM-MVS by applying images obtained using the proposed method, and then investigating the comparisons between the surface elevations. The accuracy of the resulting DSM was evaluated through a comparison of these models with the results from the RTK-GNSS survey data. It was confirmed that the proposed method could provide a sufficiently accurate DSM. The DSM was applied to the topography data of a numerical calculation to reproduce the local flow structures around the vegetation patches. The results demonstrated the advantages of using such precise topography information.

Keywords: SfM-MVS, pole camera, field observation, microtopography, riparian vegetation

1. INTRODUCTION

Excessive overgrowth of the riparian vegetation has been one of the key issues for river management in Japan over the last 30 to 40 years. Several existing studies proposed mechanisms that illustrate the expansion of the vegetated regions around river channels, and they suggested that the early stage of vegetation overgrowth is produced by the entrapment of the fine sediment materials by the pioneering herbaceous plant on disturbed sandbars (Harada et al., 2015). During the aforementioned beginning stages, spatial scales of the evolution of the topography are restricted to a relatively small scale. Because of this reason, it is necessary to precisely evaluate the evolution of such micro-scale topography in order to reveal the vegetation processes. One of the most powerful tools that can be used to tackle these points is an operation of the unmanned aerial vehicle (UAV) to acquire aerial photographs from which the Structure from Motion-Multi View Stereo (SfM-MVS) techniques are applied. Currently, these techniques are widely used because of the portability of the equipment and the feasibility of the operation. However, the current legal environment for UAV operation has globally changed due to security reasons, and restricted areas for UAV operation are expected to consistently expand hereafter. The overgrowth of riparian vegetation is commonly observed in the urban areas of Japan and the expecting legal restriction of the UAV operation may adversely affect future research activities. Because previously mentioned obstacle, this study proposed an alternative method to capture images for the SfM-MVS, in which a remote-controlled camera mounted on top of a 7 m telescopic pole was used. The Digital Surface Model (DSM) of the specific microtopography on the Shonai River was generated by using the actual images that were captured by the pole camera. The DSM was then applied to calculate the local two-dimensional flow structures. Hydraulic influences on the transport of the relatively fine sediment around the topography were evaluated through the observations of sediment distributions at the same site.

2. OBSERVATION SITE

The observation site of this study was one of the sandbars located on the Shonai River in Japan, around 28 km upstream from the mouth of the river. Figure 1 shows the exact location of the site. Sediments that were deposited on the sandbar were excavated in 2012 to obtain a flat surface. The purpose of the project was to produce a low and flat plane where the surface materials were expected to be disturbed during the relatively

small-scale flood events. Our research team began observing the evolution of the landscape on this site in 2016 and conducted field observations at intervals of several months. Figure 2 shows the ortho-rectified images of the observation period (described later). Figure 3 shows the hydrograph of the water level at the gauging station near the site, and the observation dates of this study from 2011 to 2017. The site landscape had been constantly changing through several flood events during this period, and the characteristics of this site were described as one gravel surface region upstream of the bar, and the other overgrown vegetational surface region downstream (Figure 4). Typical diameters of the bed materials representing each region are around 10 mm for the upstream gravel region (coarse sand to gravel, and close to the submerged channel bed material) and about 0.1 mm to 2 mm (silt to sand) for the downstream vegetated region. One of our existing studies (Akahori et al., 2018) evaluated the large-scale flow structures and the sediment transport mechanisms of this reach using numerical models. Their results show that the upstream gravel region has been maintained by the deposition tendency of the gravel materials during flood events. On the contrary, the downstream vegetated region did not show this same tendency, and the surface materials had not been intensively disturbed throughout the flood events. For this reason, the relatively fine materials (sand and silt) had been trapped in the downstream vegetated region.

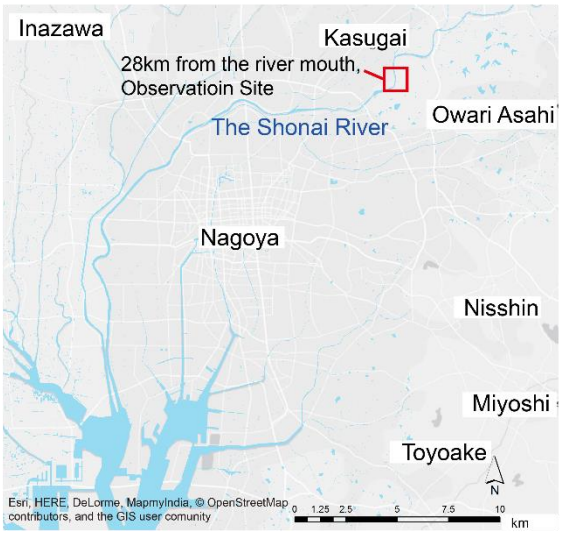

Figure 1. Observation site of the study (28 km upstream from the river mouth of the Shonai River)

Figure 2. Ortho-rectified images of the site during the observation period (a calculation area and conditions are illustrated in the image on 07/29 and 08/11/2016.)

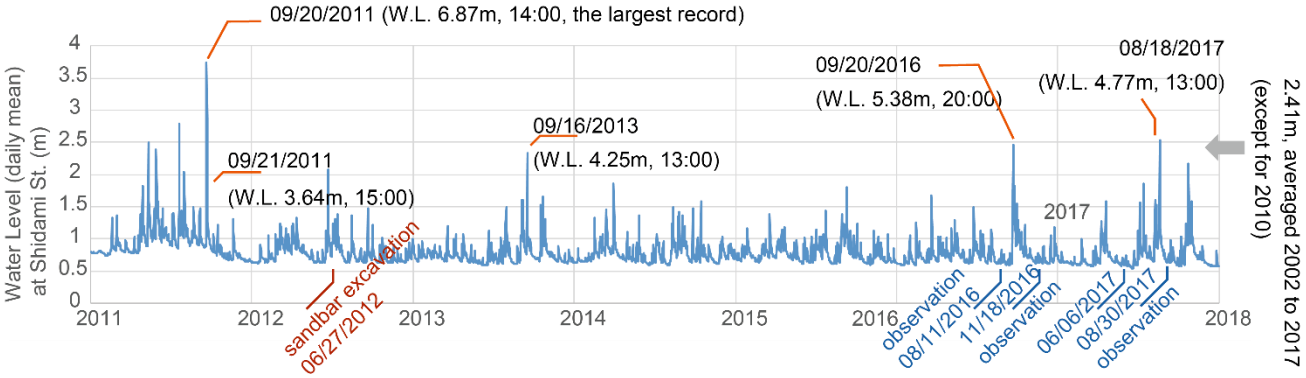

Figure 3. Hydrograph of the water level at the gauging station near the site, Shidami St., and the observation dates

Figure 4. Surface appearance of the observation site (Left: gravel surface region upstream of the bar. Right: vegetated surface region downstream).

3. RESEARCH PROCEDURES

3.1 Field observations

Observation items for this study were classified into two groups; one was for the microtopography survey and the other was for the sediment material research. The characteristics of the former group were the image acquisition obtained by the high mounted pole-camera method and the point survey using the RTK-GNSS, and the latter was characterized by sediment sampling for the surface materials.

The “pole-camera” method that was employed for this study was originally proposed in the field of the active fault research (Goto, 2015). The left image of Figure 5 shows the state of the photo shoot for this method. This method requires two operators and the specific setup of a camera, in which a remote-controlled camera (Sony, ILCE-QX1L) is mounted on top of a 7-m telescopic pole (Promate, E-4867). One of the camera operators needs to retain the pole vertically and rotate both the pole and himself at the same location, while the other operator stands beside the pole and captures images using a remote controller (Sony, RM-LVR2), paying attention to overlapping images and the inclusion of markers. The markers mentioned above must be deployed at the ground control point (GCP). The RTK-GNSS (Sokkia, GSX2) was used to obtain locations of the GCM. There were approximately 20 images for each of the 20–35 shooting locations of this study. Thus, the total number of images for all observations was approximately 400 to 700. Respectively, there were 10–20 GCP markers. The SfM-MVS technique was then applied to the images obtained using the above method in order to generate the DSM and the ortho-rectified image of the microtopography. The commercially available SfM system (Agisoft, PhotoScan Professional edition, Ver. 1.2.6) was used for this purpose. The right image in Figure 5 shows the wireframe graphic of the DSM of the downstream vegetated region at the site obtained by following the procedure described above. Figure 6 shows the plots between the elevation values of the randomly observed points by the RTK-GNSS and those at the same location points in the DSM. Figure 6 illustrates that the elevation of the DSM shows a reasonable agreement with the RTK-GNSS. The errors between those values were mostly less than 20 cm, which was close to the accuracy standards of Guidelines for creating 3D electronic

maps of rivers and watersheds by aerial laser, proposed by the Japanese Ministry of Land, Infrastructure, Transport and Tourism (MLIT).

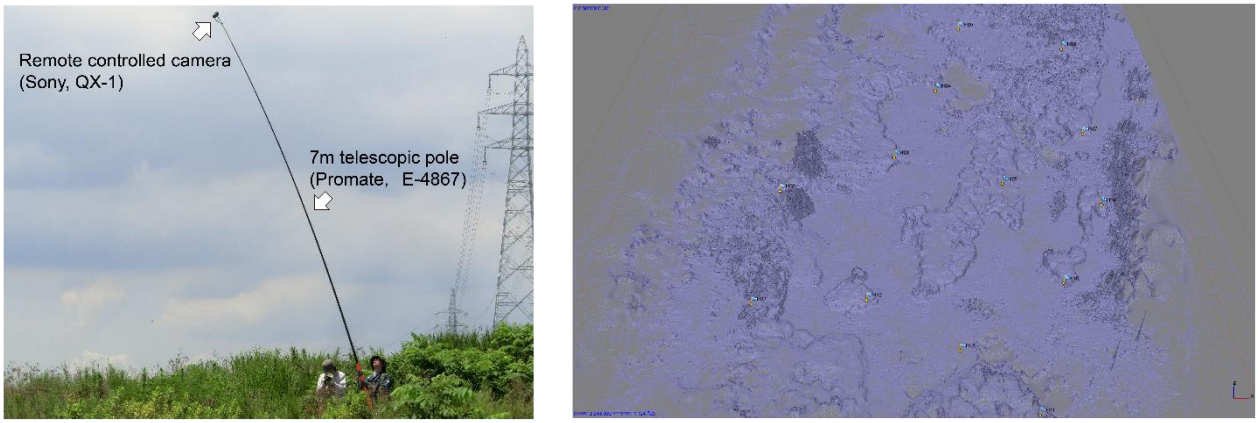

Figure 5. Procedure of the "pole camera" method (Left: state of photo shoot by using a pole camera. Right: wire frame image of the DSM obtained by the SfM-MVS employing images captured by the pole-camera method).

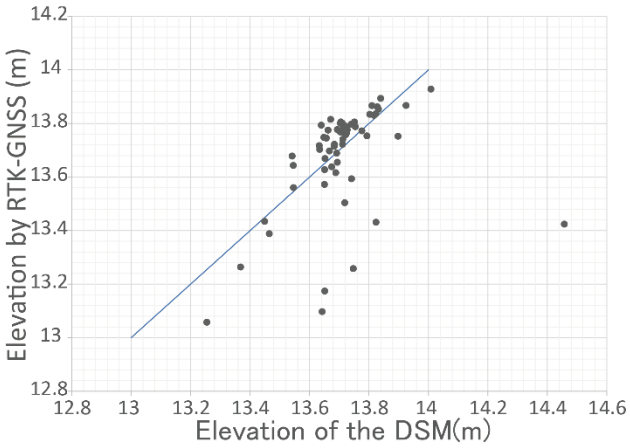

Figure 6. Plots between the elevation values of the randomly observed points by the RTK-GNSS and those of the same location points of the DSM

The surface materials of the site were manually sampled. The particle distributions of the sampled sediment were investigated by an external agency following a specific method for particle size distribution of soils (JIS A 1204).

3.2 Numerical calculation

In order to figure out the relationship between the flow structures and the mechanisms of fine sediment transport at this site, a two-dimensional flow was numerically calculated. The maximum discharge at this section was estimated to be 1500 m^3/s on September 20th in 2016 during the observation period. However, in this study, it was focused on the relatively high-frequency of small-scale flood events that were expected to gently transport fine sediments to vegetated regions. Therefore, the estimated discharge on September 9th in 2015 was used as the boundary condition. This flood was assumed to be the last event before observations on July 29th in 2016. The discharge was assumed to be around 225 m^3/s, considering the recent observation results of the discharge and the water level at the adjacent gauging station. Also, the DSM previously described was used as the topographic data of the 2-dimensional numerical analysis for this study. A rectangular grid system was applied to this calculation, and the grid sizes were 40 cm for both downstream and cross-stream directions. The image taken on July 29th and October 11th in 2016 (Figure 2) shows that the largest upstream sandbar regions divided the flow into the main and secondary channels. It was assumed that 1/3 of the total discharge flowed into the secondary channel as a result of the preliminary study; thus, the discharge at the upstream boundary was set as 75 m^3/s for this study. The numerical model used for this calculation was the customized version of Nays 2D of iRIC 2.1. (Shimizu, 2013).

The hydraulic characteristics related to the sediment transport mechanism in the resulting calculation were evaluated by comparing them with the observed particles distribution results. For this purpose, τ was calculated first at each grid by applying velocity magnitude and water depth to the calculation (Equation 1). Where τ is the local shear stress, U is the velocity magnitude, h is the water depth, n_m is Manning's coefficient, ρ is the water density, and g is the gravitational acceleration. The local friction velocity $u*$ was calculated in Equation 2 by substituting τ obtained above.

$$\tau = \rho g h^{-(\frac{1}{3})} {n_m}^2 U^2 \quad (1)$$

$$u* = \sqrt{\tau/\rho} \quad (2)$$

The threshold of sediment to be transported as suspended-load motions are commonly assumed by the ratio of the friction velocity ($u*$) to the particle settling velocity (w_s). When the ratio of $u*$ to w_s exceeds 1, it is assumed that the fine particles retain the suspended-load motion and do not contact with the bed surface. Analogous to this evaluation, the ratio of the velocity magnitude in submerged vegetation region to w_s was used as the threshold for the fine sediment deposition in this study. The friction velocity ($u*$) itself was obtained by using the above procedure, however, may not be appropriate when a grid is covered by herbal vegetation. In order to consider these types of scenarios, the near bed velocity on a vegetated grid, $u_{vegetation}$, was calculated (Equation 3). Around a submerged vegetation region, the vertical velocity distribution is able to be illustrated by the diagram of Figure 7 (Poggi et al., 2004). Equation 3 aimed to calculate the velocity magnitude in region 1 (wake zone) shown in Figure 7. Here, I_e is the local energy slope that was inversely obtained by the calculated result of Equation 1 ($\tau = \rho g h$), C_D is the drag coefficient (C_D = 1.0), and the degree of vegetated density is $a_s = nd/s^2$, where n is the number of vegetation, d is its diameter, and s is the side length of an observed area. The assumed value was a_s = 3.0 by considering the existing field studies. Here, 1-mm sand particles were supposed to represent the fine particles at this site. This estimated local threshold was compared with the observed particle distributions.

$$u_{vegetation} = \sqrt{2 g I_e / (C_D a_s)} \quad (3)$$

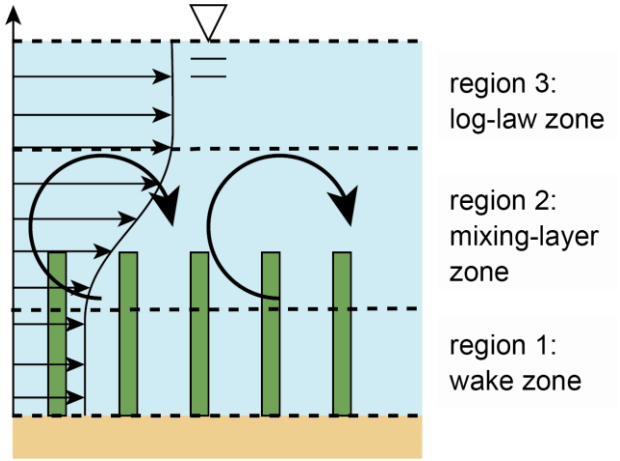

Figure 7. Vertical velocity distribution in a submerged vegetation area

4. RESULTS

4.1 Field observation

The left image of Figure 8 shows the details of the ortho-rectified image of the downstream vegetated region on July 29, 2016. The sediment sampling locations were also pointed out in the left image of Figure 8. The right image of Figure 8 shows the results of the particle distribution analyses of these samples. The results show that the particle distributions were able to be classified into two groups as the existing study stated; one being the fine sediment group and the other being the coarse material. The markers on Figure 8 are colored according to the particle size shown in the right image of Figure 8. The color becomes magenta when it's 60% passing size, D_{60}, of the sample exceeds 2 mm and the others become light green.

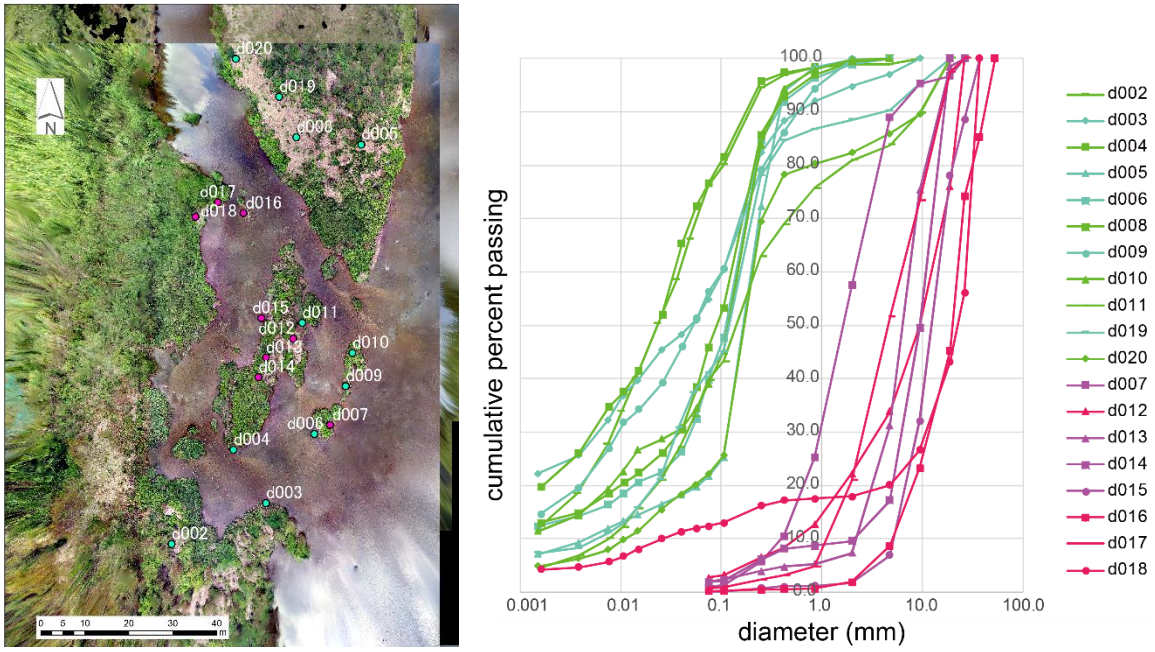

Figure 8. Particle distribution of sampled sediment (Left: sampling location. Right: particle distributions)

4.2 Numerical calculation

Figure 9 shows the contour graphics of the depth, and the velocity magnitude which were achieved at the end of the calculation time. The results show that several narrow channels run through the spaces between the vegetated mounds in this region. Comparing those contour graphics and the markers in Figure 8, we can assume that the particle size relates to the spatial distribution of the velocity magnitude rather than that of the depth.

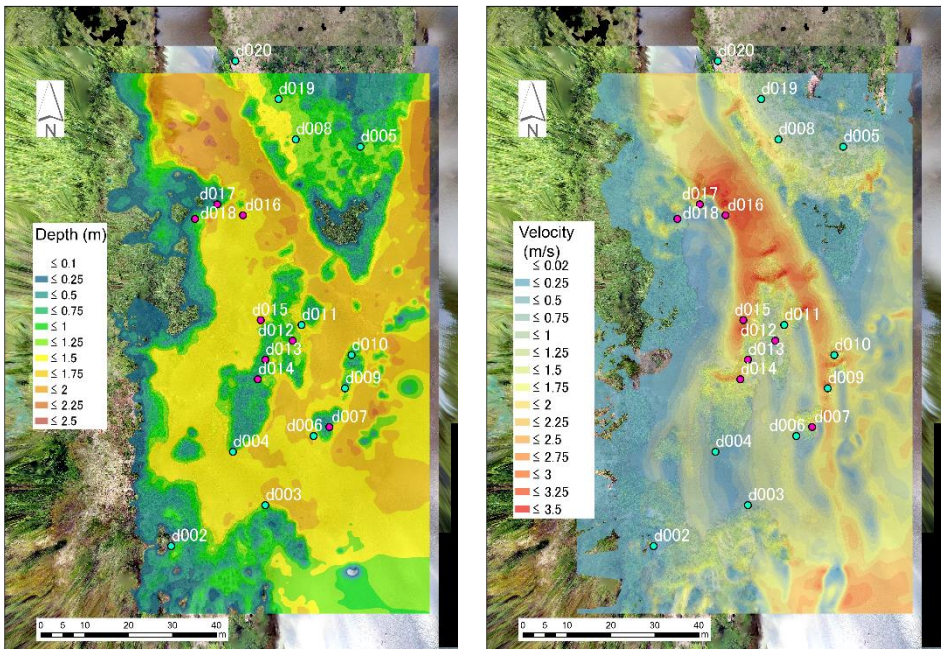

Figure 9. Contour graphics of the calculation result (Left: water depth. Right: flow velocity magnitude)

In order to clarify the influence of the hydraulic characteristics on the calculation result, the ratio of $u_{vegetation}$ to w_s was evaluated. The result is shown in the contour graphic of Figure 10. Here, the regions where the ratio $u_{vegetation}$ to w_s was less than 1 are not colored (translucent). Conversely, the colored plots denote the regions where the 1-mm particles were transported as suspended sediment. These particles are not supposed be in contact with the channel bed. Furthermore, the relatively fine materials (represented by the 1-mm particle) are not considered as trapped in the vegetation region in these colored areas because they remain entrained by the flow structures, such as wake flows or turbulence generated in the mixing layer zone. Comparing marker color to this result, most of the magenta markers were located in the areas of the colored contours. As described above, the magenta markers represent the location which was covered by relatively coarse materials. The result is consistent with the assumption that the region where the ratio of $u_{vegetation}$ to w_s exceeds 1 cannot deposit the fine sediments.

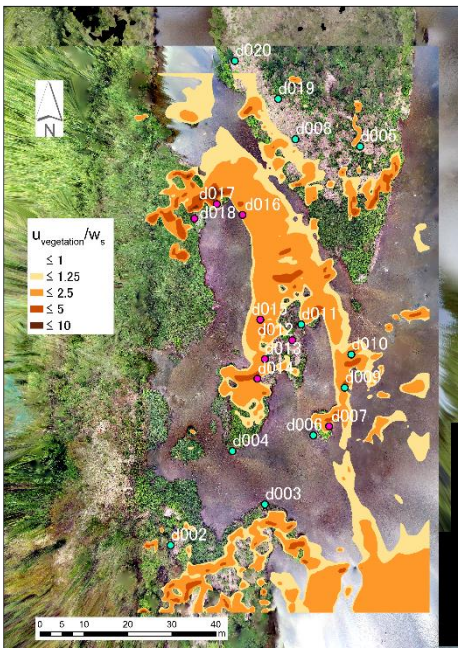

Figure 10. Contour graphics of the calculation result (the ratio of $u_{vegetation}$ to w_s)

5. CONCLUSIONS

In this study, an alternative method to capture images for the SfM-MVS was proposed, in which a remote-controlled camera mounted on a telescopic pole was used. The method was applied to our field observations on the Shonai River in order to investigate the evolution of microtopography and the riparian herbaceous vegetation. The elevation of the resulting DSM showed strong agreement with the RTK-GNSS survey data. The DSM was applied to a numerical calculation to reproduce the local flow structures around the vegetation patches. The calculated result was used to investigate the hydraulic properties of vegetated regions that have an influence on the fine sediment transport mechanisms. The estimated regions that did not have fine sediment deposits were relatively consistent with the location where coarse materials were sampled.

ACKNOWLEDGMENTS

This work was supported by JSPS KAKENHI Grant Number JP19K04625.

REFERENCES

Akahori, R., Toyoda, T., and Matsuura, R. (2018). A study on evolution of riparian vegetation and topography during a short period by applying SfM-MVS technique, *Journal of Japan Society of Civil Engineers Ser. B1 (Hydraulic Engineering)*, Vol. 74 (2018), No. 4, pp. I_553-I_558. (in Japanese)

Goto, H. (2015). Mapping of Fault Geomorphology Using "Structure from Motion - Multi - Video Stereo" Photogrammetry with Old / Hi-view Aerial Photography, *Active Fault Research*, No. 42, pp. 73-83. (in Japanese)

Harada, M., Nagayama, S., Oishi, T., and Kayaba, Y. (2015). Microtopography formation after flood-channel excavation in Ibi-River, *Journal of Japan Society of Civil Engineers Ser. B1 (Hydraulic Engineering)*, Vol. 71 (2015), No. 4, pp. I_1171-I_1176. (in Japanese)

Poggi, D., Porpotato, A., Ridolfi, L., Albertson, J. D. and Katul, G. G. (2004). The Effect of Vegetation Density on Canopy Sub-layer Turbulence, *Boundary-Layer Meteorology*, Vol.111, pp.565-587.

Shimizu, Y., Inoue, T., Hamaki, T. and Iwasaki, T. (2013). iRIC Software Nays2D Solver Manual, Retrieved from https://i-ric.org/en/download/nays2d-solver-manual/